6.7 SHORTWAVE AND LONGWAVE TOP-OF-ATMOSPHERE RADIATIVE FLUX ESTIMATION FROM THE CLOUDS AND THE EARTH'S RADIANT ENERGY SYSTEM INSTRUMENT

Norman G. Loeb[1], Seiji Kato[1], Konstantin Loukachine[2], Natividad Manalo-Smith[3]
[1]Hampton University/NASA Langley Research Center, Hampton, VA

[2]Science Applications International Corporation, Hampton, Virginia
[3]Analytical Services and Materials, Hampton, Virginia

1. INTRODUCTION

One of the largest uncertainties in global climate models is the representation of how clouds and aerosols influence the Earth's radiation budget at the surface, within the atmosphere and at the top of the atmosphere. Because of the uncertainty in cloud-aerosol-radiation interactions, model predictions of climate change vary widely from one model to the next. In order to understand the reason for these discrepancies and to identify key areas where climate models can be improved, global observations are needed. The two Clouds and the Earth's Radiant Energy System (CERES) satellite instruments aboard the Terra spacecraft provide highly accurate shortwave (SW), longwave (LW) and window (WN) radiance measurements and top-of-atmosphere (TOA) radiative flux estimates globally at 20-km spatial resolution. These data, together with coincident cloud and aerosol properties inferred from the Moderate Resolution Imaging Spectrometer (MODIS), provide a consistent cloud-aerosol-radiation dataset for studying the critical role that clouds and aerosols play in modulating the radiative energy flow within the Earth-atmosphere system.

One of the challenges involved in producing radiation datasets from satellites is the need to convert the radiance measurements at a given sun-Earth-satellite configuration to outgoing reflected solar and emitted thermal top-of-atmosphere (TOA) radiative fluxes. To estimate TOA fluxes from measured CERES radiances, one must account for the angular dependence in the radiance field, which is a strong function of the physical and optical characteristics of the scene (e.g. surface type, cloud fraction, cloud/aerosol optical depth, cloud phase), as well as the illumination angle. Because the CERES instrument can rotate in azimuth as it scans in elevation, it acquires data over a wide range of angles. Consequently, one can construct angular distribution models (ADMs) for radiance-to-flux conversion from the CERES measurements. Furthermore, since CERES and MODIS are on the same spacecraft, the ADMs can be derived as a function of MODIS-based scene type parameters that have a strong influence on radiance anisotropy.

This summary provides a brief overview of the methodology and validation results for a new set of global CERES ADMs developed from two years of CERES measurements on the Terra spacecraft. We also provide a summary of the uncertainties in both instantaneous and regional mean TOA radiative fluxes for clear and all-sky conditions over ocean, land, desert and snow surfaces. Also provided are comparisons of regional mean SW TOA fluxes from the new CERES ADMs with fluxes from the CERES ERBE-like product, which applies the algorithms developed during the Earth Radiation Budget Experiment (ERBE) to CERES data.

Corresponding author address: Norman G. Loeb
Mail Stop 420 NASA Langley Research Center, Hampton, VA 23681-0001; e-mail: n.g.loeb@larc.nasa.gov.

2. OBSERVATIONS

The Terra spacecraft, launched on December 18th, 1999, carries two identical CERES instruments: Flight Models 1 (FM-1) and 2 (FM-2). Terra is in a descending sun-synchronous orbit with an equator crossing time of 10:30 a.m. local time. The CERES instrument is a scanning broadband radiometer that measures filtered radiances in the SW (wavelengths between 0.3-5 μm), total (TOT) (wavelengths between 0.3-200 μm) and WN (wavelengths between 8-12 μm) regions. On Terra, CERES has a spatial resolution of approximately 20 km (equivalent diameter). One of the unique features of CERES is its ability to scan in either a fixed, rotating or programmable azimuth plane scan mode. Operationally, one CERES instrument is placed in a crosstrack scan mode to optimize spatial sampling for time-space averaging (Young et al., 1998), while the second instrument is either in a rotating azimuth plane (RAP), alongtrack or programmable azimuth plane (PAP) scan mode. In RAP mode, the instrument scans in elevation as it rotates in azimuth, thus acquiring radiance measurements from a wide range of viewing configurations. In PAP mode, CERES is programmed to collect measurements for a specific field campaign, for intercalibration with other instruments, or to augment sampling in specific viewing geometries. The nominal schedule is to operate the second CERES instrument in alongtrack mode every fifteen days and in RAP mode the remainder of the time.

To construct ADMs for Terra, 24 months (March 2000-February 2002) of the CERES Terra Edition2A Single Scanner Footprint TOA/Surface Fluxes and Clouds (SSF) product (Geier et al., 2001) are used. The CERES SSF product combines CERES radiances and fluxes with scene information inferred from coincident Moderate Resolution Imaging Spectroradiometer (MODIS) measurements (Barnes et al., 1998) and meteorological fields based on 4-D assimilation data. Cloud properties on the CERES Terra SSF product are inferred from MODIS pixel measurements using algorithms described in Minnis et al. (2003). Aerosol properties are determined from two sources: i) by applying the algorithm of Ignatov and Stowe (2002); and ii) directly from the MOD04 aerosol product (Remer et al., 2004). For Terra Edition2A SSF, meteorological fields on the SSF are from the Global Modeling and Assimilation Office (GMAO)'s Goddard Earth Observing System DAS (GEOS-DAS V4.0.3) product (DAO, 1996).

GMAO is running GEOS-DAS V4.0.3 without any code modifications to produce a consistent analysis over the entire CERES data record.

Accurate spatial and temporal matching of imager-derived aerosol and cloud properties with CERES broadband radiation data are obtained by accounting for the CERES point spread function (PSF) (Smith, 1994) A single footprint may contain any combination of clear area and one or two distinct cloud layers (see Fig. 1 of Loeb et al., 2003a).

3. METHODOLOGY

An ADM is a set of anisotropic factors (R) for determining the TOA flux from an observed radiance as follows:

$$\hat{F}(\theta_o) = \frac{\pi I(\theta_o,\theta,\phi)}{R(\theta_o,\theta,\phi)} \quad (1)$$

where I is the observed radiance at solar zenith angle θ_o, viewing zenith angle θ, and relative azimuth angle ϕ. R is determined empirically from two years of CERES radiance data for several scene types (Loeb et al., 2004). For a given scene type, the anisotropic factor at a given angles is:

$$R(\theta_o,\theta,\phi) = \frac{\pi L(\theta_o,\theta,\phi)}{\mathrm{M}(\theta_o)} \quad (2)$$

where L is the ADM-predicted radiance, and M is the corresponding TOA flux obtained from the following:

$$\mathrm{M}(\theta_o) = \int_0^{2\pi}\int_0^{\frac{\pi}{2}} L(\theta_o,\theta,\phi)\cos\theta\sin\theta d\theta d\phi \quad (3)$$

Tables 1 and 2 provide a summary of the CERES Terra ADM scene types for SW, LW and WN. The scene types are stratified by parameters that influence the angular dependence in the radiance field. Where appropriate, the ADMs are continuous functions of the scene type parameters. Fig. 1 shows SW ADMs for water clouds over ocean as a function of θ near the principal plane for three θ_o bins. In each θ_o interval, the liquid water clouds show well-defined peaks in anisotropy for θ = -30° to -60° and close to nadir due to the cloud glory and rainbow features, respectively. Such pronounced microphysical features were not present in ADMs developed for the ERBE (Suttles et al., 1988) and CERES TRMM (Loeb et al., 2003a) because the angular bins used to define those ADMs were much coarser than those now used for CERES Terra.

4. RESULTS

4.1 Instantaneous TOA Flux Uncertainty

In May 2003, one of the two CERES instruments on the Terra spacecraft was placed in the PAP scan mode to collect simultaneous multiangle measurements over the Atmospheric Radiation Measurement (ARM) Program's Southern Great Plains (SGP) site located at 36° 37′ N, 97° 30′ W. To test how well the CERES Terra ADMs represent the angular dependence in the instantaneous radiation

Scene Type	Description
Clear Ocean	Function of wind speed; Correction for aerosol optical depth included
Cloud Ocean	Function of cloud phase; continuous function of cloud fraction and cloud optical depth (5-parameter sigmoid)
Land & Desert Clear	1° regional monthly ADMs using analytical function of TOA BRDF (Ahmad and Deering, 1992)
Land & Desert Cloud	Function of cloud phase; continuous function of cloud cover and cloud optical depth; uses 1°-regional clear-sky BRDFs to account for background albedo
Permanent Snow	Cloud fraction, surface brightness, cloud optical depth
Fresh Snow	Cloud Fraction, surface brightness, snow fraction, cloud optical depth
Sea-Ice	Cloud fraction, surface brightness, ice fraction, cloud optical depth

Table 1 SW ADM scene types.

Scene Type	Description
Clear Ocean, Land, Desert	Ocean, Forest, Cropland/Grass, Savanna, Bright Desert, Dark Desert, precipitable. water, lapse rate, skin temperature
Clouds Over Ocean, Land, Desert	Function of precipitable. water, skin temperature., surface-cloud temperature. difference; continuous function of parameterization involving cloud fraction, cloud and surface emissivity, surface and cloud temperature
Permanent Snow Fresh Snow Sea-Ice	Each a function of cloud fraction, surface temperature, surface-cld temperature difference

Table 2 LW and WN ADM scene types.

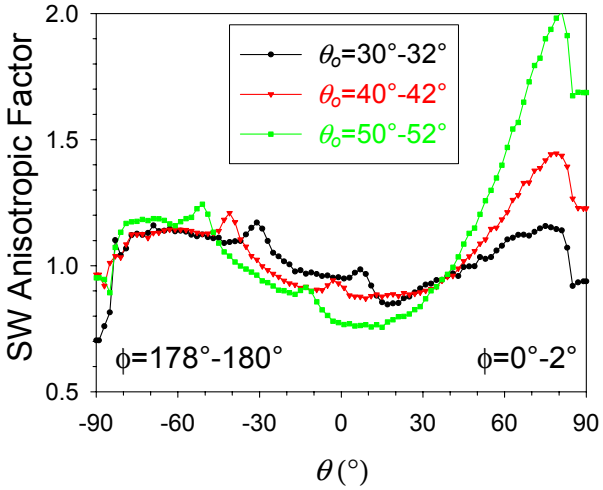

Figure 1 SW ADMs for water clouds over ocean as a function of satelline viewing geometry.

field for overcast conditions, four overcast days covering the entire range of relative azimuth angles from 0°-360° were selected. The viewing geometry on these days is shown in Fig. 2a. The observed and ADM-predicted radiances normalized by the average radiance of each day are shown in Fig. 2b. For these scenes, the CERES Terra ADMs closely reproduce the instantaneous anisotropy in the observed radiances. In terms of error in instantaneous SW TOA flux, these differences correspond to relative errors ranging from 1.5% to 4%. Table 3 summarizes instantaneous TOA flux error estimates for a much larger sample drawn from 80 days when CERES was in the alongtrack scan mode. Terra results are compared with those using the CERES TRMM ADMs applied to Terra observations. The Terra ADMs show modest improvements relative to TRMM, except over clear land, and clear and all-sky snow, where errors in the Terra SW fluxes are 1.5-3 times smaller than TRMM.

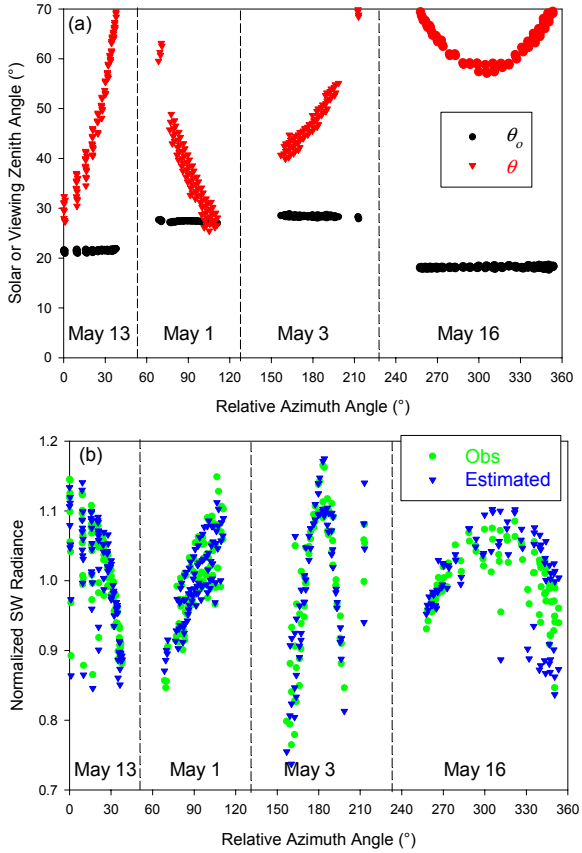

Figure 2 (a) CERES viewing geometry and (b) observed and estimated overcast TOA normalized SW radiance over the Southern Great Plains ARM site for selected days in May 2003.

4.2 Regional Mean TOA Flux Errors

Regional mean TOA fluxes uncertainties are estimated by comparing ADM-derived all-sky TOA fluxes averaged over 10°x10° latitude-longitude regions with TOA fluxes determined by direct integration of the measured radiances for the same regions (Loeb et al., 2003b). Results, summarized in Table 4, indicate that regionally averaged TOA fluxes are generally within 1 W m-2 of direct integration fluxes both in the SW and LW regions. Regional maps show larger SW TOA flux errors (reaching 5 W m-2) over high-albedo targets in the polar regions during the summertime when insolation is high. In the LW, daytime TOA flux errors reach +3 W m-2 over snow-covered mountainous regions and-5 W m-2 over Antarctica in DJF.

Region	S_o W m^{-2}	Terra ADMs W m^{-2} (%)		TRMM ADMs W m^{-2} (%)	
		Clear	All-sky	Clear	All-sky
Tropics	1150	5.2 (2.2)	14.3 (5.1)	7.7 (3.5)	14.3 (5.8)
Midlat	870	4.2 (3.0)	13.5 (3.9)	7.3 (5.6)	13.7 (4.1)
Polar	540	12.8 (4.3)	17.3 (5.9)	37.0 (11.7)	29.2 (9.8)

Table 3 Estimated instantaneous SW TOA flux uncertainty for CERES Terra ADMs.

	Season	Avg Diff (W m-2)	RMS Diff (W m-2)
SW (Day)	DJF	-0.42	0.89
SW (Day)	JJA	-0.56	0.96
LW (Day)	DJF	-0.04	0.93
LW (Day)	JJA	0.26	0.82
LW (Night)	DJF	-0.10	1.34
LW (Night)	JJA	0.24	1.02

Table 4 Estimated regional 24-h average TOA flux error due to CERES Terra ADMs.

4.3 Monthly Mean TOA Flux Comparisons with ERBE

Regional distributions of SW TOA flux differences between the CERES Terra ERBE-like (ES8) and SSF instantaneous TOA flux products (no diurnal averaging) are shown in Figs. 3a-b. Over most of the ocean, clear-sky ES8 SW TOA fluxes are larger than SSF fluxes by 15-20 W m^{-2} (or ≈5-7 W m^{-2} with diurnal averaging). This large discrepancy is mainly due to cloud contamination in the ES8 results. Clear scenes on the ES8 are identified from the CERES SW and LW radiances using a Maximum Likelihood Estimation Technique (Wielicki and Green, 1985). With this approach, identifying small-scale cumulus within the CERES field-of-view is quite difficult because of the low thermal contrast of these scenes with the clear ocean background. By utilizing MODIS, which has a much higher spatial-resolution than CERES, cloud contamination is greatly reduced, and TOA fluxes are much lower compared to ES8. Large SW TOA flux differences also occur over Antarctica and over

snow-covered areas in the Northern Hemisphere. These differences are primarily due to (i) different snow maps in the two products; (ii) poor scene identification (clear vs cloud) over snow for ERBE; and (iii) ADM differences.

Differences in all-sky TOA fluxes (Fig. 3b) are largest in a narrow band near 30°S. This is likely associated with ADM differences at the solar zenith angles corresponding to these latitudes in December. Substantial SW TOA flux differences are also evident off the coast of Antarctica, a region primarily covered with sea-ice. TOA fluxes in this region are highly sensitive to scene identification because SW anisotropy varies substantially depending upon whether a scene is identified as open ocean, sea-ice, or cloud, all of which can occur in that region.

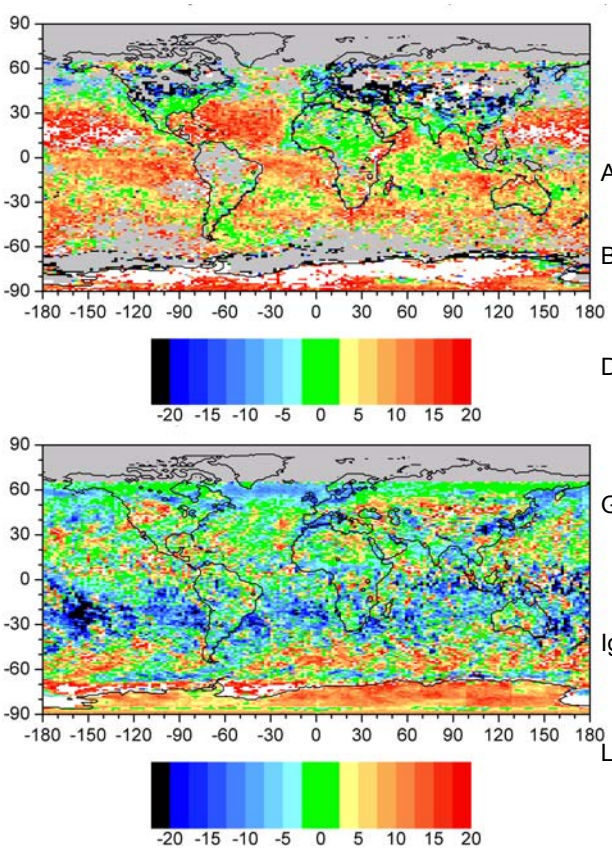

Figure 3 ERBE-like (ES8) minus SSF average SW TOA flux difference for December 2001. (a) clear sky; (b) all-sky.

5. CONCLUSIONS

New global ADMs for CERES Terra show improvements over ADMs developed for TRMM, particularly over polar regions. Instantaneous TOA flux errors are estimated to be between 2%-4% for clear scenes and approximately 5% in all-sky conditions. Regional 24-h TOA flux RMS errors are estimated to be < 1 W m-2.

The large clear and all-sky SW TOA flux differences between the ERBE-like and SSF products have important implications for studies that use ERBE-like TOA fluxes for comparing model and observed cloud radiative forcing (CRF). Since clear-sky SW TOA fluxes from the ERBE-like product are generally larger than SSF fluxes over ocean (where SW cloud radiative forcing is most pronounced), the CRF should be larger from the SSF product. The increase in CRF will be particularly large in those regions where the ERBE-like all-sky TOA fluxes are smaller than SSF (e.g., near 30°S in Fig. 3b). In those regions, we expect SW cooling by clouds to increase by 3-5 W m^{-2} (diurnally averaged) compared to ERBE.

ACKNOWLEDGEMENTS

This research is funded by the Clouds and the Earth's Radiant Energy System (CERES) project under NASA grant NNL-04AA26G.

REFERENCES

Ahmad, S. P., and D. W. Deering, 1992: A simple analytical function for bidirectional reflectance. *J. Geophys. Res.*, **97**, 18,867-18,886.

Barnes, W.L.,T.S. Pagano, and V.V. Salomonson, 1998: Prelaunch characteristics of the Moderate Resolution Imaging Spectroradiometer (MODIS) on EOS-AM1, *IEEE Trans. Geosci. Remote Sens.*, **36**, 1088–1100.

DAO, 1996: Algorithm Theoretical Basis Document for Goddard Earth Observing System Data Assimilation System (GEOS DAS) with a focus on version2. [Available online from http://dao.gsfc.nasa.gov/subpages/atbd.html].

Geier, E.B., R. N. Green, D. P. Kratz, P. Minnis, W. F. Miller, S. K. Nolan, and C. B. Franklin, 2001: Single satellite footprint TOA/surface fluxes and clouds (SSF) collection document. [available on-line from http://asd-www.larc.nasa.gov/CERES ASDceres.html.]

Ignatov, A. and L. L. Stowe, 2002: Aerosol retrievals from individual AVHRR channels: I. Retrieval algorithm and transition from Dave to 6S radiative transfer model. *J. Atmos. Sci.*, **59**, 313-334.

Loeb, N.G., S. Kato, K. Loukachine, and N.M. Smith, 2004: Angular distribution models for top-of-atmosphere radiative flux estimation from the Clouds and the Earth's Radiant Energy System instrument on the Terra Satellite. Part I: Methodology, *J. Ocean. Atmos. Tech.*, (submitted).

Loeb, N.G., N.M. Smith, S. Kato, W.F. Miller, S.K. Gupta, P. Minnis, and B. A. Wielicki, 2003a: Angular distribution models for top-of-atmosphere radiative flux estimation from the Clouds and the Earth's Radiant Energy System instrument on the Tropical Rainfall Measuring Mission Satellite. Part I: Methodology, *J. Appl. Meteor.*, 42, 240-265.

Loeb, N.G., K. Loukachine, N. M. Smith, B. A. Wielicki, and D. F. Young, 2003b: Angular distribution models for top-of-atmosphere radiative flux estimation from the Clouds and the Earth's Radiant Energy System instrument on the Tropical Rainfall Measuring Mission

Satellite. Part II: Validation, *J. Appl. Meteor*., 42, 1,748-1,769.

Minnis, P., D. F. Young, S. Sun-Mack, P. W. Heck, D. R. Doelling, and Q. Trepte, 2003: "CERES Cloud Property Retrievals from Imagers on *TRMM*, *Terra*, and Aqua" Proc. SPIE 10th International Symposium on Remote Sensing: Conference on Remote Sensing of Clouds and the Atmosphere VII, Barcelona, Spain, September 8-12, 37-48.

Remer, L. A., Y. J. Kaufman, D. Tanré, S. Mattoo, D. A. Chu, J. V. Martins, R.-R. Li, C. Ichoku, R.C. Levy, R.G. Kleidman, T.F. Eck, E. Vermote and B. N. Holben, 2004: The MODIS aerosol algorithm, products and validation. *J. Atmos. Sci*. (submitted).

Smith, G. L., 1994: Effects of time response on the point spread function of a scanning radiometer. *Appl. Opt*., **33**, 7031-7037.

Suttles, J.T., B.A. Wielicki, and S. Vemury, 1992: Top-of-atmosphere radiative fluxes: Validation of ERBE scanner inversion algorithm using Nimbus-7 ERB data. *J. Appl. Meteor*., **31**, 784-796.

Wielicki, B.A., and R.N. Green, 1989: Cloud identification for ERBE radiation flux retrieval. *J. Appl. Meteor*., **28**, 1133-1146.

Young, D. F., P. Minnis, D. R. Doelling, G. G. Gibson, and T. Wong, 1998: Temporal interpolation methods for the Clouds and the Earth's Radiant Energy System (CERES) experiment. *J. Appl. Meteor*., **37**, 572-590.